

Optomagnetic non-thermal modification of the ferromagnetic resonance

Nika Gribova,^{1,2,*} Anatoly Zvezdin,³ Shixun Cao,⁴ and Vladimir Belotelov^{1,5}

¹*Russian Quantum Center, Moscow 121205, Russia*

²*Moscow Institute of Physics and Technology (National Research University), Dolgoprudny 141701, Russia*

³*Prokhorov General Physics Institute of the Russian Academy of Sciences, Moscow 119991, Russia*

⁴*Department of Physics, Materials Genome Institute, Institute for Quantum Science and Technology, Shanghai University, Shanghai 200444, China*

⁵*Lomonosov Moscow State University, Moscow 119991, Russia*

(Dated: May 15, 2026)

We investigate the photoinduced shift of the ferromagnetic resonance (FMR) frequency in magnets caused by the inverse Cotton-Mouton effect (ICME) under linearly polarized light. Using a Lagrangian description of magnetization dynamics, we derive the equations of motion, and obtain analytical expressions for the resonance frequency in both in-plane and out-of-plane equilibrium configurations. The theory shows that the FMR frequency depends on the polarization angle and propagation direction of light, with ICME producing a frequency shift that can dominate over thermal effects. The analytical results agree well with numerical simulations and with available experimental data for bismuth-substituted yttrium iron garnet, enabling estimation of the ICME contribution. These findings demonstrate that linearly polarized light can be used to control ferromagnetic resonance through magneto-optical effects.

INTRODUCTION

Over the past several decades, the interaction between light and spins in magnetically ordered materials has emerged as a focal point of condensed matter research [1–5]. Initial investigations primarily utilized femtosecond laser pulses to induce both thermal [7–9] and non-thermal [10] modifications of spin states. Non-thermal mechanisms are driven by photoinduced magnetic anisotropy [7, 11] or optomagnetic phenomena, including the inverse Faraday and Cotton-Mouton effects (IFE and ICME, respectively). These interactions facilitate advanced functionalities such as ultrafast all-optical switching [7, 9, 11–13] and the coherent excitation of spin waves [14, 15].

While transient pulse excitation is prominent, continuous-wavelaser irradiation also offers a viable pathway for spin manipulation. Early research focused on photomagnetic data storage [16, 17], largely relying on localized laser heating to modulate magnetization and anisotropy—a principle now industrialized via Heat-Assisted Magnetic Recording [18, 19]. However, such thermal effects necessitate significant optical absorption to drive electronic transitions. In transparent dielectrics, specifically rare-earth iron garnets, absorption-mediated heating is minimized, allowing non-thermal, inverse magneto-optical effects to dominate. These include the Inverse Faraday Effect, driven by circularly polarized light [1, 20], and the Inverse Cotton-Mouton Effect, triggered by linearly polarized light [21–23].

Ferromagnetic resonance lies in roots of many magnetic experiments and applications and is governed by the effective field entering the Kittel [24, 25] relation and therefore depends on external bias. The FMR in garnet

films is modulated by external field magnitude and orientation [26], film thickness [27–30], chemical composition [31–33], and temperature-dependent magnetic properties [34–37]. Furthermore, tuning is achieved through elastic strain [29, 30, 38], electric-field coupling [39–41], and light-induced anisotropy changes ranging from steady-state shifts to ultrafast precessional triggering [8, 42, 43].

Dynamic control of ferromagnetic resonance frequency via external stimuli is a critical objective, with optical modulation offering high precision. The Inverse Cotton-Mouton Effect facilitates non-thermal magnetic anisotropy modification within a material’s transparency range. In ferrimagnetic garnets like $\text{Y}_3\text{Fe}_5\text{O}_{12}$ (YIG) and bismuth-substituted variants (BiYIG), ICME enables efficient magnetization precession triggering via linearly polarized light, often surpassing the efficiency of the inverse Faraday effect or photo-induced anisotropy [3, 44]. Furthermore, in antiferromagnets such as orthoferrites and NiO, ICME-driven coherent magnon excitation by linearly polarized pulses is orders of magnitude stronger than circular polarization-driven effects [2, 45]. These findings indicate that ICME can be used for fundamentally shifting FMR frequency through optical modulation of the effective magnetic field.

As the experimental foundation for our research, we employ the results obtained by [46], where a key experiment relevant to the present problem was carried out. While the experimental data are of significant value, the theoretical description is not complete. In this work, a consistent and rigorous theory is formulated, providing full agreement with the experimental observations from [46] and given additional insights into light mediated non-thermal control of FMR.

In this work, we investigate the dependence of the FMR frequency on the in-plane orientation of the polarization of light at room temperature. Experimental data indicate that ICME provides the main contribu-

* gribova.ni@phystech.edu

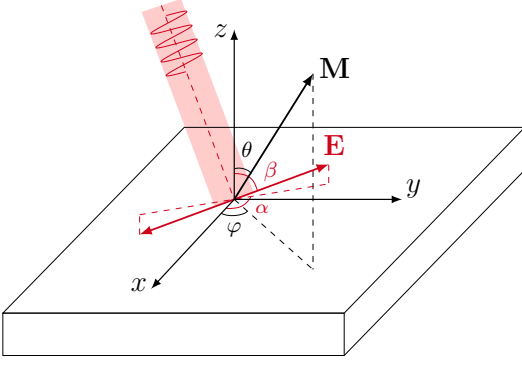


Figure 1: Ferromagnetic film with uniaxial magnetic anisotropy in the external magnetic field H_{ext} along x axis.

tion to the polarization-dependent frequency shift, that dominates photothermal contribution to shift of FMR frequency. We analyze the observed frequency shifts in terms of anisotropy fields generated by ICME and their relation to static anisotropies.

THEORY

Let's consider an iron garnet thin film in an external in-plane magnetic field $\mathbf{H} = (H, 0, 0)$. The Cartesian coordinate system is chosen to get z -axis out-of-plane and x -axis along the external magnetic field (Fig. 1). The film exhibits uniaxial magnetic anisotropy in the cases of easy-axis, while the effects associated with cubic crystallographic anisotropy are not taken into account. The sample is illuminated by linearly polarized light characterized by the electric field $\mathbf{E} = E_0(\sin \beta \cos \alpha, \sin \beta \sin \alpha, \cos \beta)$, which is parameterized by two angles α and β . Here, β denotes the angle of deviation of the polarization of incident light from the normal of the film, while α represents the rotation of the in-plane polarization projection relative to the x -axis.

To describe the dynamics of magnetization in this system we employ the Lagrangian formalism. The spherical coordinates are chosen as the polar and azimuthal angles (θ, φ) of the magnetization $\mathbf{M} = M(\sin \theta \cos \varphi, \sin \theta \sin \varphi, \cos \theta)$ in Cartesian system. The Lagrangian of the system is constructed from the kinetic term and the potential energy.

$$\mathcal{L} = -\frac{M}{\gamma} \dot{\phi} \cos \theta - U_a - U_z - U_d - U_{cm} \quad (1)$$

The total potential energy U includes several contributions: Zeeman energy U_z due to the static magnetic field, uniaxial magnetocrystalline anisotropy U_a , demagnetization energy U_d , spin-photon interaction energy described by the inverse Cotton-Mouton effect U_{cm} . The exchange energy was omitted, since we consider the film to be in a monodomain state. The above energy contributions can

be written in spherical coordinates as

$$U_a = -K_u \cos^2 \theta, \quad (2)$$

$$U_z = -MH \sin \theta \cos \varphi, \quad (3)$$

$$U_d = 2\pi M^2 \cos^2 \theta, \quad (4)$$

$$U_{cm} = K_{cm} \left[\cos 2\beta + \cos 2\theta + 3 \cos 2\beta \cos 2\theta \right. \\ \left. + \sin^2 \beta \sin^2 \theta (4 \cos 2\alpha \cos 2\varphi + \sin 2\alpha \sin 2\varphi) \right. \\ \left. + \cos(\alpha - \varphi) \sin 2\beta \sin 2\theta \right], \quad (5)$$

where derivation of Cotton-Mouton energy is given in detail in Appendix B.

Constructing the Euler-Lagrange equations based on the Lagrangian with the energy terms presented in Eqs. (2-5), one obtains the equations of magnetization motion for $\theta(t)$ and $\varphi(t)$.

$$\dot{\theta} = -\gamma H \sin \varphi \quad (6)$$

$$- \omega_{cm} \left[\sin \theta \sin^2 \beta (\sin 2\alpha \cos 2\varphi - 4 \cos 2\alpha \sin 2\varphi) \right. \\ \left. + \cos \theta \sin 2\beta \sin(\alpha - \varphi) \right]$$

$$\dot{\varphi} = \cos \theta \left(\omega_u - 2\omega_{cm}(1 + 3 \cos 2\beta) - \frac{\gamma}{\sin \theta} H \cos \varphi \right) \quad (7)$$

$$+ \omega_{cm} \left[\cos \theta \sin^2 \beta (4 \cos 2\alpha \cos 2\varphi + \sin 2\alpha \sin 2\varphi) \right. \\ \left. + \frac{\cos 2\theta}{\sin \theta} \sin 2\beta \cos(\alpha - \varphi) \right]$$

where γ is a gyromagnetic ratio, $\omega_{cm} = \frac{2\gamma K_{cm}}{M}$, $\omega_u = \frac{2\gamma(K_u - 2\pi M^2)}{M}$ and $K_{cm} = (a_1 - a_2)M^2 E_0^2 / 8$ with constants a_1, a_2 , representing two possible ICME energy contributions admitted by the symmetry group of the system (Appendix B). These equations describe the precessional dynamics of magnetization determined by uniaxial anisotropy and external fields of a magnetic field and linearly polarized light, when the system is perturbed from an equilibrium position.

The equilibrium state ($\frac{\partial U}{\partial \theta} = 0, \frac{\partial U}{\partial \varphi} = 0$ with $\omega_{cm} = 0$) is determined by the value of the uniaxial anisotropy and the external magnetic field. Here we will consider in detail the case when initially the magnetization is alongside the external magnetic field: $\theta_0 = \pi/2, \varphi_0 = 0$. For the magnetic film with the "easy-axis" anisotropy ($K_u > 2\pi M^2$) it is realized if $H > \frac{2K_u}{M} - 4\pi M$. If the uniaxial anisotropy of the magnetic film is "easy-plane" type ($K_u < 2\pi M^2$) then any external magnetic field along x -axis provides this equilibrium state. The case of the out-of-plane magnetization equilibrium position is described in the Appendix C.

Therefore, to linearize Eqs. (6-7) it is convenient to pass small angles $\theta_1, \varphi_1 \ll 1$ as $\varphi = \varphi_0 + \varphi_1$ and $\theta = \theta_0 + \theta_1$. Taking into account terms up to the first order in θ_1, φ_1 , as numerical modeling indicates that this is sufficient to accurately describe the system, we get the following linearized equation for the free magnetization

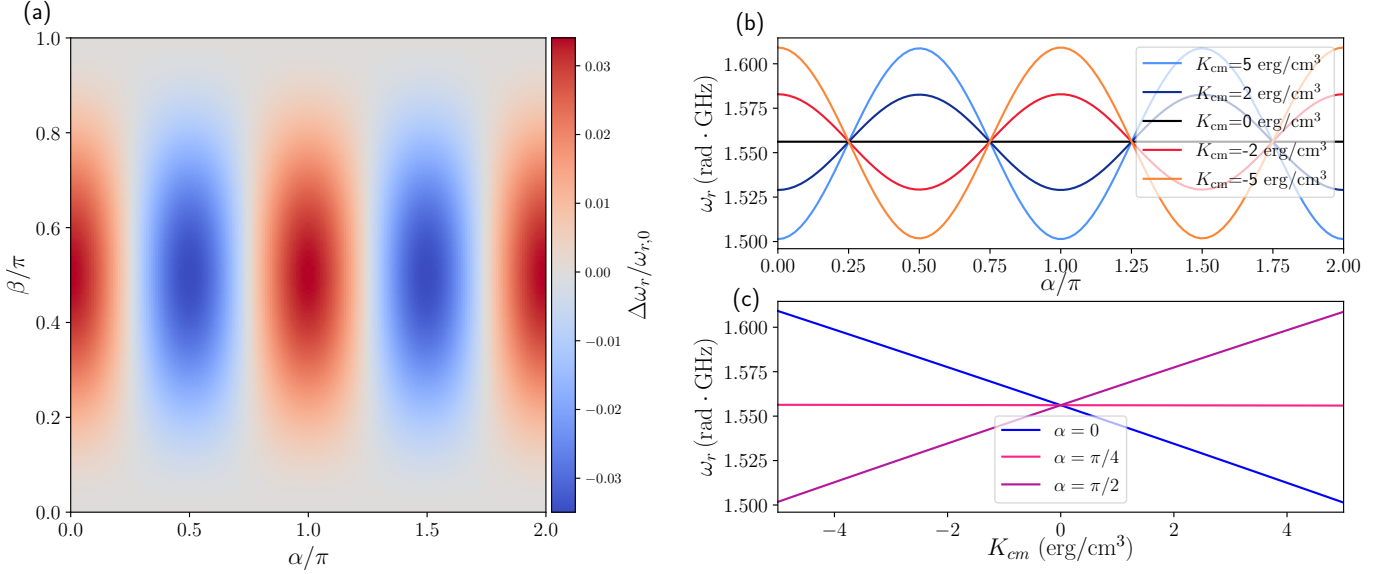


Figure 2: The resonant frequencies dependence on the parameters α , β and K_{cm} with equilibrium position in-plane with $K_u - 2\pi M^2 < 0$. (a) The colormap with fixed parameter $K_{cm} = -5$ erg/cm³ illustrates analytical expression for $\Delta\omega_r/\omega_{r,0}$ derived from the Eq. 12, where $\omega_{r,0} = \omega_r(K_{cm} = 0)$ and $\Delta\omega_r = \omega_r - \omega_{r,0}$. (b) Dependence of ω_r at normal light incidence ($\beta = \pi/2$) on the polarization angle α for several values of ICME parameter K_{cm} . (c) Dependence of ω_r at normal light incidence on K_{cm} for $\alpha = 0, \pi/4, \pi/2$.

precession

$$\dot{\theta}_1 = -\omega_1\varphi_1 + \omega_3\theta_1 + \omega_5, \quad (8)$$

$$\dot{\varphi}_1 = \omega_2\theta_1 + \omega_4\varphi_1 + \omega_6, \quad (9)$$

where $\omega_1 = \gamma H - 8\omega_{cm} \cos 2\alpha \sin^2\beta$, $\omega_2 = \gamma H - \omega_u + 2\omega_{cm}(1 + 3\cos 2\beta - 2\cos 2\alpha \sin^2\beta)$, $\omega_3 = -\omega_4 = \omega_{cm} \sin \alpha \sin 2\beta$, $\omega_5 = -\omega_{cm} \sin 2\alpha \sin^2\beta$ and $\omega_6 = -\omega_{cm} \sin 2\beta \cos \alpha$. These linearized equations 8, 9 can be solved exactly under the initial conditions $\theta_1(0)$ and $\varphi_1(0)$, assuming $\frac{\omega_{cm}}{\gamma H_x} \ll 1$ we have

$$\varphi_1(t) = \frac{1}{\omega_r^2} \left[\Omega_1^2 + \Omega_2^2 \cos \omega_r t + \omega_r \Omega_3 \sin \omega_r t \right], \quad (10)$$

$$\theta_1(t) = \frac{1}{\omega_r^2} \left[\Omega_4^2 + \Omega_5^2 \cos \omega_r t + \omega_r \Omega_6 \sin \omega_r t \right], \quad (11)$$

$$\omega_r = \sqrt{\omega_1\omega_2 - \omega_3^2}, \quad (12)$$

where ω_r is the resonant frequency, $\Omega_1^2 = \omega_2\omega_5 - \omega_3\omega_6$ and $\Omega_4^2 = \omega_3\omega_5 - \omega_1\omega_6$ are determined only by the parameters of the system, $\Omega_2^2 = \varphi_1(0)\omega_r^2 - \Omega_1^2$, $\Omega_3 = \theta_1(0)\omega_2 - \varphi_1(0)\omega_3 + \omega_6$, $\Omega_5^2 = \theta_1(0)\omega_r^2 - \Omega_4^2$ and $\theta_1(0)\omega_3 - \varphi_1(0)\omega_1 + \omega_5$ are determined by the system and the initial conditions of magnetization precession $\theta_1(0)$ and $\varphi_1(0)$. The magnitude and polarization of a linearly polarized electric field affects not only the magnitude of the Cotton–Mouton effect but also induces a frequency shift. The Eq. 12 is in good agreement with Kittel formula (Appendix A)

In the case of normal incidence of light ($\beta = \pi/2$) the Eq. 12 is simplified ($\omega_3 = \omega_4 = \omega_6 = 0$) and resonant frequency becomes $\omega_r = \sqrt{\omega_1\omega_2}$.

PROPERTIES OF THE OPTOMAGNETIC SHIFT OF FMR

Fig. 2 demonstrates dependence on α , β and K_{cm} . The parameters of system are selected for bismuth substituted iron garnet film BiY₂Fe_{4.4}Sc_{0.6}O₁₂ [46]: $H = 8$ Oe, $4\pi M = 1830$ Oe, $\gamma = 1.76 \times 10^{-5}$ ps⁻¹Oe⁻¹ and $K_u = 61.6 \times 10^3$ erg cm⁻³. For this set of parameters $K_u - 2\pi M^2 = -70.6 \times 10^3$ erg cm⁻³ the in plane equilibrium condition is satisfied.

Fig. 2(a) presents the relative resonant frequency change $\Delta\omega_r/\omega_{r,0}$ calculated by Eq. 12, where $\omega_{r,0} = \omega_r(K_{cm} = 0)$ and $\Delta\omega_r = \omega_r - \omega_{r,0}$. The largest influence of light on FMR appears for normal incidence ($\beta = \pi/2$).

The dependence of ω_r on the polarization angle α at normal light incidence is plotted in Fig. 2(b) for several values of ICME parameter K_{cm} . For selected parameters, the peak values of ω_r correspond to the angles around $\alpha = 0, \pi/2, \pi, 3\pi/2$, where polarization of light is either parallel or perpendicular to the equilibrium position of magnetization. On the contrary, if α is nearly $\pi/4, 3\pi/4, 5\pi/4, 7\pi/4$, then there is no change in FMR frequency and $\omega_r = \omega_{r,0}$.

Larger K_{cm} produces a stronger shift of FMR. Fig. 2(c) demonstrates that the effect gets stronger for increasing K_{cm} and the frequency shift is almost linear in K_{cm} , i.e. in the incident light intensity.

In this section we apply the developed theory to describe the experimental results obtained in [46] where dependence of ω_r on light polarization was measured. Fig. 3 presents a theoretical description of the experimental data (black dots) by Eq. (12) (solid curve). The

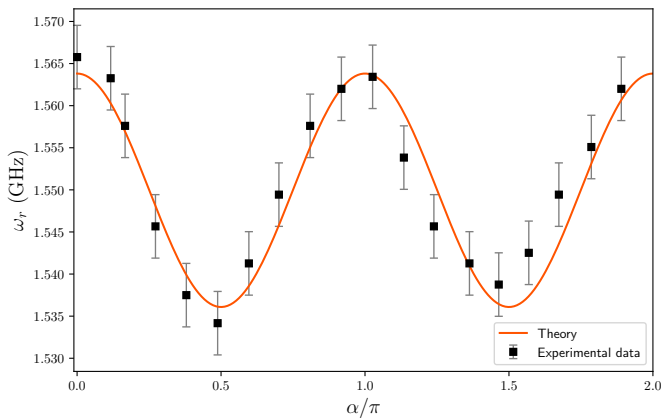


Figure 3: Dependence of the FMR frequency on the polarization direction α of the light wave at $T = 300$ K. A constant magnetic field $H_x = 8$ Oe is applied. The light beam with power $P = 25$ mW makes an angle of $\approx 5^\circ$ with the normal to the sample plane. Experimental data points (black dots) are taken from article [46]. The solid theoretical curve is calculated according to equation 12 using the experimental parameters.

magnetic parameters are taken the same as in the beginning of section. The best correspondence is achieved for $K_{cm} = -1.25$ erg cm $^{-3}$. Since in the experiment light beam power was 25 mW one can find $a_1 - a_2 = -3.1 \times 10^{-7}$ /Oe 2 , which value is the same order as presented in [47].

CONCLUSION

The study demonstrated that linearly polarized CW light leads to the shift of FMR frequency by the inverse Cotton-Mouton effect. The theoretical consideration was

based on the Lagrangian formalism considering magnetization dynamics in the magnetic potential taking into account a contribution from the ICME. The latter was derived from the group theory analysis.

The FMR frequency shift is almost linear with light intensity. It depends on the polarization of light with respect to the equilibrium magnetization state. If initial magnetization is along the in-plane external magnetic field then the maximum influence of light takes place for the light polarization either parallel or perpendicular to the equilibrium magnetization. The case when initial magnetization is out-of-plane was considered in Appendix C.

The dependence of the resonance frequency shift on varying system parameters was further analyzed. Two equilibrium configurations were examined: one with the magnetization lying in the film plane and another with the magnetization oriented out of the plane. For both cases, the frequencies obtained from nonlinear numerical simulations were systematically compared with those predicted by the linearized model, showing quantitative agreement.

Finally, the theoretical predictions were confronted with available experimental results. The comparison confirmed the applicability of the developed theory and enabled the determination of the ICME constants for the studied sample.

ACKNOWLEDGMENTS

This work was financially supported by Russian Science Foundation (Project No. 23-62-10024) in part related to electromagnetic modeling of the spin dynamics. N.I.G. and V.I.B. also acknowledge support from the Foundation for the Advancement of Theoretical Physics and Mathematics “BASIS” (Project No. 25-1-1-49-4) for analytical theoretical studies.

Appendix A: Kittel formula for FMR

Kittel formula for the ferromagnetic resonance frequency

$$\omega_{\text{fmr}}^2 = \frac{\gamma^2}{M^2 \sin^2 \theta_0} \left(\frac{\partial^2 U}{\partial \theta^2} \frac{\partial^2 U}{\partial \varphi^2} - \left(\frac{\partial^2 U}{\partial \theta \partial \varphi} \right)^2 \right)_{\theta=\theta_0, \varphi=\varphi_0} \quad (\text{A1})$$

is obtained from the second derivatives of the total energy U [24, 25, 48]. The ferromagnetic resonance frequency calculated ω_{fmr} using the Kittel formula A1 coincides with the previously obtained value ω_r (Eq. 12). This confirms the validity of the derivation and the consistency of theoretical description of the system’s dynamics.

Appendix B: Derivation of Cotton-Mouton energy

A system of iron garnet thin film is considered, where a Cartesian system is introduced: the film lies in the x, y plane and its normal coincides with the z -axis. The sample is illuminated by linearly polarized light characterized

by the electric field $\mathbf{E} = E_0(\sin\beta\cos\alpha, \sin\beta\sin\alpha, \cos\beta)$, which is parameterized by two angles α and β . Here, β denotes the angle of deviation of the incident light from the normal to the film, while α represents the rotation of the polarization plane relative to the x -axis. The spherical coordinates are chosen as the polar and azimuthal angles (M, θ, φ) of the magnetization vector \mathbf{M} (in Cartesian coordinate system $\mathbf{M} = M(\sin\theta\cos\varphi, \sin\theta\sin\varphi, \cos\theta)$).

When analyzing a physical system, the first step is to identify the symmetry group of its Hamiltonian, that is, the set of transformations that leave the Hamiltonian invariant [49]. In our work, we consider a system with uniaxial anisotropy, meaning that there exists a single distinguished direction along the z -axis.

The crystallographic class of type $\infty\infty$ corresponds to the symmetry class of infinitely extended cylindrical objects [50]. The first ∞ denotes an infinite rotational axis along a certain direction, while the second ∞ indicates the existence of an infinite set of equivalent directions perpendicular to this axis. In other words, the object possesses cylindrical symmetry. From the tensor of the Cotton–Mouton coefficients [50], one can derive the expression [49] for the Cotton–Mouton energy as

$$U_{CM} = a_1(M_x^2 E_x^2 + M_y^2 E_y^2 + M_z^2 E_z^2) + a_2\left(M_x^2(E_z^2 + E_y^2) + M_y^2(E_z^2 + E_x^2) + M_z^2(E_x^2 + E_y^2)\right) + \quad (B1)$$

$$+ \frac{a_1 - a_2}{2}\left(M_x M_y E_x E_y + M_x M_z E_x E_z + M_z M_y E_z E_y\right),$$

where z axis is directed along the easy axis of the uniaxial anisotropy. Writing equations in spherical coordinates with $\mathbf{M} = M(\sin\theta\cos\varphi, \sin\theta\sin\varphi, \cos\theta)$ and $\mathbf{E} = E_0(\sin\beta\cos\alpha, \sin\beta\sin\alpha, \cos\beta)$, omitting constants we get

$$U_{CM} = \frac{a_1 - a_2}{8} M^2 E_0^2 \left[\cos 2\beta + \cos 2\theta + 3 \cos 2\beta \cos 2\theta + \sin^2 \beta \sin^2 \theta (4 \cos 2\alpha \cos 2\varphi + \sin 2\alpha \sin 2\varphi) \right. \quad (B2)$$

$$\left. + \cos(\alpha - \varphi) \sin 2\beta \sin 2\theta \right].$$

In the case $\beta = \pi/2$, which is equivalent to the normal incidence of light (along the z axis), we have

$$U_{CM} = K_{cm} \left[-2 \cos 2\theta + \sin^2 \theta (4 \cos 2\alpha \cos 2\varphi + \sin 2\alpha \sin 2\varphi) \right], \quad (B3)$$

where $K_{cm} = \frac{a_1 - a_2}{8} M^2 E_0^2$

Appendix C: The case of out-of-plane equilibrium magnetization state

In this section, we consider the case when the equilibrium position with $\omega_{cm} = 0$ of magnetization lies out of the (xy) plane. This situation is realized in the case of an easy axis, when $K_u > 2\pi M^2$, and the external magnetic field $|\mathbf{H}| < \frac{2K_u}{M} - 4\pi M$. The equilibrium position of magnetization is determined by $\theta_0 = \arcsin(|\mathbf{H}| / (\frac{2K_u}{M} - 4\pi M))$ and $\varphi_0 = 0$, since we consider without limitation generality \mathbf{H} along the x axis.

The same linearization procedure around the equilibrium position has been performed for the case $\theta_0 \neq \pi/2$. where $\kappa_1, \kappa_2, \kappa_3$ and κ_4 are determined under the assumption $4\kappa_1\kappa_2 > (\kappa_3 - \kappa_4)^2$. This result coincides with the formula 12 in the case of $\theta_0 = \pi/2$.

In this case, the general form of the equations remains the same, but the coefficients have a more form. The angles that determine the orientation of the magnetization can be represented as $\phi = \phi_0 + \phi_1$ and $\theta = \theta_0 + \theta_1$ with small deviations from the ground state $\theta_1, \phi_1 \ll 1$. Taking into account terms up to the first order in θ_1, ϕ_1 , as numerical modeling indicates that this is sufficient to accurately describe the system, we derive the Euler-Lagrange linearized equations from equations 6 and 7

$$\dot{\theta}_1(t) = -\kappa_1\varphi_1 + \kappa_3\theta_1 + \kappa_5, \quad (C1)$$

$$\dot{\varphi}_1(t) = \kappa_2\theta_1 + \kappa_4\varphi_1 + \kappa_6, \quad (C2)$$

where $\kappa_1 = \gamma H_x - \omega_{cm}(\cos\theta_0\cos\alpha\sin 2\beta + 8\sin\theta_0\cos 2\alpha\sin^2\beta)$, $\kappa_3 = \omega_{cm}(\sin\theta_0\sin\alpha\sin 2\beta - \cos\theta_0\sin 2\alpha\sin^2\beta)$, $\kappa_5 = -\omega_{cm}(\cos\theta_0\sin\alpha\sin 2\beta + \sin\theta_0\sin 2\alpha\sin^2\beta)$, $\kappa_2 = \omega_{cm}\left[(-2 + \cos 2\theta_0)\frac{\cos\theta_0}{\sin^2\theta_0}\cos\alpha\sin 2\beta + 2\sin\theta_0(1 + 3\cos 2\beta - 2\cos 2\alpha\sin^2\beta)\right] - \omega_u\sin\theta_0 + \frac{\gamma H_x}{\sin^2\theta_0}$, $\kappa_4 = \omega_{cm}(2\cos\theta_0\sin 2\alpha\sin^2\beta + \frac{\cos 2\theta_0}{\sin\theta_0}\sin\alpha\sin 2\beta)$ and $\kappa_6 = \omega_{cm}\left[\frac{\cos 2\theta_0}{\sin\theta_0}\cos\alpha\sin 2\beta - 2\cos\theta_0(1 + 3\cos 2\beta - 2\cos 2\alpha\sin^2\beta)\right] + \omega_u\cos\theta_0 - \frac{\cos\theta_0}{\sin\theta_0}\gamma H_x$. These linearized equations can be solved under the initial

conditions $\theta_1(0)$ and $\varphi_1(0)$, that have the form

$$\varphi_1(t)\xi_1^2 = \xi_2^2 + e^{\frac{\omega_3+\omega_4}{2}t} \left[(\varphi_1(0)\xi_1^2 - \xi_2^2) \cos \omega_r t + \frac{\sin \omega_r t}{2\omega_r} (2\theta_1(0)\kappa_2\xi_1^2 - \varphi_1(0)(\kappa_3 - \kappa_4)\xi_1^2 + \kappa_2\kappa_5(\kappa_3 + \kappa_4) + \kappa_6(2\kappa_1\kappa_2 - \kappa_3^2 + \kappa_3\kappa_4)) \right], \quad (C3)$$

$$\theta_1(t)\xi_1^2 = -\xi_3^2 + e^{\frac{\omega_3+\omega_4}{2}t} \left[(\theta_1(0)\xi_1^2 + \xi_3^2) \cos \omega_r t - \frac{\sin \omega_r t}{2\omega_r} (2\varphi_1(0)\kappa_1\xi_1^2 - \theta_1(0)(\kappa_3 - \kappa_4)\xi_1^2 + \kappa_5(-2\kappa_1\kappa_2 - \kappa_3\kappa_4 + \kappa_4^2) + \kappa_1\kappa_6(\kappa_3 + \kappa_4)) \right] \quad (C4)$$

$$\omega_r^2 = \kappa_1\kappa_2 - \frac{(\kappa_3 - \kappa_4)^2}{4}, \quad (C5)$$

where $\xi_1^2 = \kappa_1\kappa_2 + \kappa_3\kappa_4$, $\xi_2^2 = \kappa_2\kappa_5 - \kappa_3\kappa_6$ and $\xi_3^2 = \kappa_4\kappa_5 + \kappa_1\kappa_6$.

The resonant frequency for this case can be represented as an analytical function:

$$\omega_r^2 = \kappa_1\kappa_2 - \frac{(\kappa_3 - \kappa_4)^2}{4}, \quad (C6)$$

-
- [1] AV Kimel, A Kirilyuk, PA Usachev, RV Pisarev, AM Balbashov, and Th Rasing. Ultrafast non-thermal control of magnetization by instantaneous photomagnetic pulses. *Nature*, 435(7042):655–657, 2005.
- [2] AM Kalashnikova, AV Kimel, RV Pisarev, VN Gridnev, Andrei Kirilyuk, and Th Rasing. Impulsive generation of coherent magnons by linearly polarized light in the easy-plane antiferromagnet febo 3. *Physical review letters*, 99(16):167205, 2007.
- [3] Isao Yoshimine, Takuya Satoh, Ryugo Iida, Andrzej Stupakiewicz, Andrzej Maziewski, and Tsutomu Shimura. Phase-controllable spin wave generation in iron garnet by linearly polarized light pulses. *Journal of applied physics*, 116(4), 2014.
- [4] A Stupakiewicz, Krzysztof Szerenos, MD Davydova, KA Zvezdin, AK Zvezdin, Andrei Kirilyuk, and AV Kimel. Selection rules for all-optical magnetic recording in iron garnet. *Nature communications*, 10(1):612, 2019.
- [5] Denis M Krichevsky, Vladislav A Ozerov, Alexandra V Bel'kova, Daria A Sylgacheva, Andrey N Kalish, Svetlana A Evstigneeva, Alexander S Pakhomov, Tatiana V Mikhailova, Sergey D Lyashko, Alexander L Kudryashov, et al. Spatially inhomogeneous inverse faraday effect provides tunable nonthermal excitation of exchange dominated spin waves. *Nanophotonics*, 13(3):299–306, 2024.
- [6] Nika Gribova, Anatoly Zvezdin, and Vladimir Belotelov. Peculiarities of spin dynamics excitation by magnetic field of a high-frequency electromagnetic pulse. *arXiv preprint arXiv:2509.26528*, 2025.
- [7] TA Ostler, J Barker, RFL Evans, RW Chantrell, U Atxitia, O Chubykalo-Fesenko, S El Moussaoui, LBPJ Le Guyader, E Mengotti, LJ Heyderman, et al. Ultrafast heating as a sufficient stimulus for magnetization reversal in a ferrimagnet. *Nature communications*, 3(1):666, 2012.
- [8] Lucile Soumah, Davide Bossini, Abdelmadjid Anane, and Stefano Bonetti. Optical frequency up-conversion of the ferromagnetic resonance in an ultrathin garnet mediated by magnetoelastic coupling. *Physical Review Letters*, 127(7):077203, 2021.
- [9] A. Frej, I. Razdolski, A. Maziewski, and A. Stupakiewicz. Nonlinear subswitching regime of magnetization dynamics in photomagnetic garnets. *Phys. Rev. B*, 107:134405, Apr 2023.
- [10] Savelli V Lutsenko, Anastasia E Khramova, Daria O Ignatyeva, Daniil V Konkov, Natalia S Kaurova, Anatoly A Syrov, Alexander L Kudryashov, Grigory N Goltsman, Vladimir N Berzhansky, and Vladimir I Belotelov. Magnetophotonic waveguide nanostructure for selective ultrafast optical excitation of high-k spin dynamics. *arXiv preprint arXiv:2408.08710*, 2024.
- [11] C. D. Stanciu, F. Hansteen, A. V. Kimel, A. Kirilyuk, A. Tsukamoto, A. Itoh, and Th. Rasing. All-optical magnetic recording with circularly polarized light. *Phys. Rev. Lett.*, 99:047601, Jul 2007.
- [12] K Vahaplar, AM Kalashnikova, AV Kimel, Denise Hinzke, Ulrich Nowak, R Chantrell, A Tsukamoto, A Itoh, A Kirilyuk, and Th Rasing. Ultrafast path for optical magnetization reversal via a strongly nonequilibrium state. *Physical review letters*, 103(11):117201, 2009.
- [13] NI Gribova, DO Ignatyeva, NA Gusev, AK Zvezdin, and VI Belotelov. Optomagnonic logic based on optical non-thermal magnetization switching in near-compensated iron-garnets. *arXiv preprint arXiv:2602.06844*, 2026.
- [14] Takuya Satoh, Yuki Terui, Rai Moriya, Boris Ivanov, Kazuya Ando, Eiji Saitoh, Tsutomu Shimura, and Kazuo Kuroda. Directional control of spin-wave emission by spatially shaped light. *Nature Photonics*, 6:662–666, 10 2012.
- [15] IV Savochkin, M Jäckl, VI Belotelov, IA Akimov, MA Kozhaev, DA Sylgacheva, AI Chernov, AN Shaposhnikov, AR Prokopov, VN Berzhansky, et al. Generation of spin waves by a train of fs-laser pulses: a novel ap-

- proach for tuning magnon wavelength. *Scientific reports*, 7(1):5668, 2017.
- [16] Yipeng Jiao and R. H. Victora. Dependence of predicted areal density on common optimization strategies for heat-assisted magnetic recording. *IEEE Magnetics Letters*, 8:1–4, 2017.
- [17] H. J. Richter, Gregory Parker, Matteo Staffaroni, Michael Grobis, and Barry C. Stipe. Heat assisted magnetic recording with laser pulsing. *IEEE Transactions on Magnetics*, 50(11):1–7, 2014.
- [18] Christoph Vogler, Claas Abert, Florian Bruckner, Dieter Suess, and Dirk Praetorius. Heat-assisted magnetic recording of bit-patterned media beyond 10 tb/in². *Applied Physics Letters*, 108(10), 2016.
- [19] Dieter Weller, Gregory Parker, Oleksandr Mosendz, Eric Champion, BC Stipe, X Wang, T Klemmer, G Ju, and A Ajan. A hamr media technology roadmap to an areal density of 4 tbit/in²/in². *IEEE Trans. Magn.*, 50:3100108, 2014.
- [20] PS Pershan. Nonlinear optical properties of solids: energy considerations. *Physical Review*, 130(3):919, 1963.
- [21] BA Zon, V Ya Kupersmidt, GV Pakhomov, and TT Urazbaev. Observation of inverse cotton-mouton effect in the magnetically ordered crystal (lu, bi) 3 (fe, ga) 5 o 12. *ZhETF Pisma Redaktsiiu*, 45:219, 1987.
- [22] Daria Popova, Andreas Bringer, and Stefan Blügel. Theory of the inverse faraday effect in view of ultrafast magnetization experiments. *Physical Review B—Condensed Matter and Materials Physics*, 84(21):214421, 2011.
- [23] Anatolii Konstantinovich Zvezdin, Roman Mikhailovich Dubrovin, and Alexey Vol'demarovich Kimel. Giant parametric amplification of the inverse cotton-mouton effect in antiferromagnetic crystals. *JETP Letters*, 119(5):363–371, 2024.
- [24] Charles Kittel. On the theory of ferromagnetic resonance absorption. *Physical review*, 73(2):155, 1948.
- [25] Charles Kittel. Ferromagnetic resonance. *Journal de Physique et le Radium*, 12(3):291–302, 1951.
- [26] Seongjae Lee, Scott Grudichak, Joseph Sklenar, CC Tsai, Moongyu Jang, Qinghui Yang, Huaiwu Zhang, and John B Ketterson. Ferromagnetic resonance of a yig film in the low frequency regime. *Journal of Applied Physics*, 120(3), 2016.
- [27] Ying Liu, Peng Zhou, Rao Bidthanapally, Jitao Zhang, Wei Zhang, Michael R Page, Tianjin Zhang, and Gopalan Srinivasan. Strain control of magnetic anisotropy in yttrium iron garnet films in a composite structure with yttrium aluminum garnet substrate. *Journal of Composites Science*, 6(7):203, 2022.
- [28] Yiheng Rao, Dainan Zhang, Huaiwu Zhang, Lichuan Jin, Qinghui Yang, Zhiyong Zhong, Mingming Li, Caiyun Hong, and Bo Ma. Thickness dependence of magnetic properties in submicron yttrium iron garnet films. *Journal of Physics D: Applied Physics*, 51(43):435001, 2018.
- [29] Jinjun Ding, Chuanpu Liu, Yuejie Zhang, Uppalaiah Erugu, Zhiyong Quan, Rui Yu, Ethan McCollum, Songyu Mo, Sheng Yang, Haifeng Ding, et al. Nanometer-thick yttrium iron garnet films with perpendicular anisotropy and low damping. *Physical Review Applied*, 14(1):014017, 2020.
- [30] Adam Krysztofik, Sevgi Özoğlu, Robert D McMichael, and Emerson Coy. Effect of strain-induced anisotropy on magnetization dynamics in y₃fe₅o₁₂ films recrystallized on a lattice-mismatched substrate. *Scientific reports*, 11(1):14011, 2021.
- [31] VV Randoshkin, VI Kozlov, V Yu Mochar, NV Vasil'eva, NA Es' kov, and Yu A Durasova. Characteristic features of ferromagnetic resonance in iron-garnet films with orthorhombic magnetic anisotropy. *Physics of the Solid State*, 41(7):1144–1148, 1999.
- [32] Ethan R Rosenberg, Kai Litzius, Justin M Shaw, Grant A Riley, Geoffrey SD Beach, Hans T Nembach, and Caroline A Ross. Magnetic properties and growth-induced anisotropy in yttrium thulium iron garnet thin films. *Advanced Electronic Materials*, 7(10):2100452, 2021.
- [33] Sreeveni Das, Rhodri Mansell, Lukáš Flajšman, Lide Yao, and Sebastiaan Van Dijken. Perpendicular magnetic anisotropy in bi-substituted yttrium iron garnet films. *Journal of Applied Physics*, 134(24), 2023.
- [34] CL Jermain, SV Aradhya, ND Reynolds, RA Buhrman, JT Brangham, MR Page, PC Hammel, FY Yang, and DC Ralph. Increased low-temperature damping in yttrium iron garnet thin films. *Physical Review B*, 95(17):174411, 2017.
- [35] M Haidar, M Ranjbar, M Balinsky, RK Dumas, Sergiy Khartsev, and Johan Åkerman. Thickness-and temperature-dependent magnetodynamic properties of yttrium iron garnet thin films. *Journal of Applied Physics*, 117(17), 2015.
- [36] MI Panin, NE Kupchinskaya, MV Bakhmetiev, RB Morgunov, VN Berzhansky, VI Belotelov, SN Polulyakh, and AI Chernov. Exploring magnetic anisotropy in garnet films at low temperatures using ferromagnetic resonance. *Journal of Applied Physics*, 137(4), 2025.
- [37] I Laulicht, JT Suss, and J Barak. The temperature dependence of the ferromagnetic and paramagnetic resonance spectra in thin yttrium-iron-garnet films. *Journal of applied physics*, 70(4):2251–2258, 1991.
- [38] Marwan Deb, Elena Popova, Michel Hehn, Niels Keller, Stéphane Mangin, and Gregory Malinowski. Picosecond acoustic-excitation-driven ultrafast magnetization dynamics in dielectric bi-substituted yttrium iron garnet. *Physical Review B*, 98(17):174407, 2018.
- [39] Rui Yu, Kang He, Qi Liu, Xucheng Gan, Bingfeng Miao, Liang Sun, Jun Du, Hongling Cai, Xiaoshan Wu, Mingzhong Wu, et al. Nonvolatile electric-field control of ferromagnetic resonance and spin pumping in pt/yig at room temperature. *Advanced Electronic Materials*, 5(3):1800663, 2019.
- [40] IV Zavislyak, MA Popov, G Sreenivasulu, and G Srinivasan. Electric field tuning of domain magnetic resonances in yttrium iron garnet films. *Applied Physics Letters*, 102(22), 2013.
- [41] Xufeng Zhang, Tianyu Liu, Michael E Flatté, and Hong X Tang. Electric-field coupling to spin waves in a centrosymmetric ferrite. *Physical review letters*, 113(3):037202, 2014.
- [42] A Stupakiewicz, A Maziewski, I Davidenko, and V Zablotskii. Light-induced magnetic anisotropy in codoped garnet films. *Physical Review B*, 64(6):064405, 2001.
- [43] F Atoneche, AM Kalashnikova, AV Kimel, A Stupakiewicz, A Maziewski, Andrei Kirilyuk, and Th Rasing. Large ultrafast photoinduced magnetic anisotropy in a cobalt-substituted yttrium iron garnet. *Physical Review B—Condensed Matter and Materials Physics*, 81(21):214440, 2010.

- [44] LQ Shen, LF Zhou, JY Shi, M Tang, Z Zheng, D Wu, SM Zhou, LY Chen, and HB Zhao. Dominant role of inverse cotton-mouton effect in ultrafast stimulation of magnetization precession in undoped yttrium iron garnet films by 400-nm laser pulses. *Physical Review B*, 97(22):224430, 2018.
- [45] Ryugo Iida, Takuya Satoh, Tsutomu Shimura, Kazuo Kuroda, BA Ivanov, Yusuke Tokunaga, and Yoshinori Tokura. Spectral dependence of photoinduced spin precession in dyfe0 3. *Physical Review B—Condensed Matter and Materials Physics*, 84(6):064402, 2011.
- [46] Sergei Nikolaevich Polulyakh, E Yu Semuk, Anatolii Konstantinovich Zvezdin, Vladimir Naumovich Berzhanskii, and Vladimir Igorevich Belotelov. Light-induced modification of the fmr spectra of a bismuth-substituted yttrium ferrite garnet film. *JETP Letters*, 115(4):196–201, 2022.
- [47] RV Pisarev, IG Sinii, NN Kolpakova, and Yu M Yakovlev. Magnetic birefringence of light in iron garnets. *Sov. Phys. JETP*, 33:1175, 1971.
- [48] H Suhl. Ferromagnetic resonance in nickel ferrite between one and two kilomegacycles. *Physical Review*, 97(2):555, 1955.
- [49] Morton Hamermesh. *Group theory and its application to physical problems*. Courier Corporation, 2012.
- [50] Shaskolskaya M.P Sirotn YuI. *Fundamentals of Crystal Physics*. Mir Publishers, Moscow, 1982.